Proceedings of the Twenty-Seventh International Pump Users Symposium
September 12-15, 2011, Houston, Texas

INFLUENCE OF IMPELLER LEADING EDGE PROFILES ON CAVITATION AND SUCTION PERFORMANCE

Ravi Balasubramanian
Hydraulics Engineer
ITT Goulds Pumps
Seneca Falls, NY, USA

Eugene Sabini
Director of Research
ITT Goulds Pumps
Seneca Falls, NY, USA

Simon Bradshaw
API Product Development Manager
ITT Goulds Pumps
Seneca Falls, NY, USA

Ravi Balasubramanian is a Hydraulics Engineer with ITT Goulds Pumps responsible for applied research and hydraulic design of engineered API process pumps. His responsibilities include development of state-of-the art simulation and modeling tools for centrifugal pump analysis and design, and cavitation prediction. Prior to joining ITT Goulds Pumps, he worked as a Research Scientist in the Aerospace Engineering Department of The Ohio State University.

Dr. Balasubramanian received his Doctorate in Computational Engineering with focus on Fluid and Thermal Sciences from Mississippi State University in 2005. He is a member of the American Institute of Aeronautics and Astronautics Fluid Dynamics Technical Committee since 2009.

Eugene P. (Gene) Sabini is the Director of Research at ITT Goulds Pumps. Mr. Sabini is responsible for applied research and hydraulic design of all new products and field re-rates. He has 43 years of experience in the pumping industry including design and development of many centrifugal pumps for the chemical, API, power utilities, and municipal industries. Before joining ITT Goulds Pumps, he was the Engineering Manager with Worthington Pumps, Harrison NJ, designing, engineering, and testing custom centrifugal pumps from both a mechanical and hydraulic standpoint.

He has authored numerous papers and holds seventeen patents. He is a recipient of The 2007 ITT Industries' Engineered for Life Lifetime Achievement award for Hydraulic Design Expertise and Innovation.

Mr. Sabini received a BSME and M.S. degree from Stevens Institute of Technology in Hoboken NJ and is a member of the International Pump Users Symposium Advisory Committee since 1999.

Simon Bradshaw is the Global API Product Development Manager for ITT Goulds Pumps, in Seneca Falls NY. His responsibilities include the design and development of new products and processes. Prior to joining ITT Goulds, he worked for both Sulzer Pumps and Weir Pumps, where he held various positions of engineering and contractual responsibility.

Mr Bradshaw has a BEng (Hons) degree (Mechanical Engineering) from Heriot Watt University. He is a registered Chartered Engineer in the UK and a member of the Institute of Engineering Designers.

ABSTRACT

The cavitation behavior and suction performance of a pump are largely influenced by the geometry at the impeller eye. A number of geometric factors at the impeller eye have an influence on cavitation, such as, the inlet and hub diameters, blade inlet angles and incidence to upstream flow, blade number and thickness, blade passage throat area, surface roughness, blade leading edge profiling, etc. In this paper, we study the influence of blade leading edge profiles, keeping all other parameters as identical, on the cavitation behavior of an impeller. Leading edge profiles such as blunt, circular, elliptic, and parabola are considered and the effect of different profiles

on cavitation inception, bubble growth, cavity length and NPSH-3% head drop performance are investigated. Experiments are performed on a cavitation visualization test rig and complemented by two-phase computational fluid dynamic (CFD) modeling and analysis.

INTRODUCTION

Cavitation is defined as the formation of vapor bubbles in a liquid where the static pressure of the liquid falls below the saturation vapor pressure of the liquid. Cavitation is accompanied by the phase change of a fluid from liquid to vapor phase and, the subsequent collapse of the vapor bubbles when the local static pressure increases above saturation pressure resulting in intense pressure waves that impact and cause material loss on the impeller. The process of cavitation in impellers can be succinctly summarized as: (i) cavitation inception - the formation of vapor bubbles near the leading edge; (ii) bubble growth and the transport of vapor cavities downstream of leading edge; and (iii) cavitation destruction and condensation - collapse of vapor bubbles when the surrounding local pressure increases above saturation pressure. Cavitation can cause serious issues to normal pump operation such as loss of material through cavitation erosion affecting impeller life, and performance deterioration accompanied by head loss.

A number of design factors influence the cavitation behavior of a pump:

(i) inlet casing (or suction volute) design

(ii) impeller geometry especially at the impeller eye, and

(iii) discharge volute design

The suction volute (or casing) design is critical to ensure that suction recirculation is minimized and the flow at the impeller eye is uniform without excessive swirl and pre-rotation. The discharge volute typically has minimal influence on the cavitation behavior near BEP operation, but, gets especially important at part load operation because of discharge recirculation traveling to the impeller inlet affecting cavitation performance. The biggest influence on the cavitation behavior of a pump is the geometry at the impeller eye. A number of geometric factors at the impeller eye have an influence on cavitation, such as, the inlet and hub diameters, blade inlet angles and incidence to upstream flow, blade number and thickness, blade passage throat area, surface roughness, blade leading edge profiling, etc.

A number of authors have over the years studied and reported the influence of some of the above factors on pump cavitation [Palgrave and Cooper., 1986, Schiavello et al., 1989, Sloteman., 1995, Hergt et. al., (1996), Dupont., 2001, Schiavello and Visser., 2008 and Gulich., 2010]. An excellent tutorial that covers all the aspects of cavitation can be found in Schiavello and Visser (2008). Palgrave and Cooper, 1986, have conducted visual studies of cavitation and present a general expression for estimating $NPSH_i$ based on inlet angle and eye diameter. Schiavello et al., 1989 have performed visual studies on a cavitation rig and compared impeller designs with different tip-to-hub shockless capacity ratios on their suction performance. Hergt et. al., (1996), have documented the suction performance of impellers for different eye diameters, vane inlet angles and number of vanes. They also studied three different leading edge contours for a prescribed profile: symmetrical tapering and asymmetrical tapering (also, commonly known as knifing) on either the suction or pressure surface of the blade to measure their impact on cavitation inception and 3%-head drop performance. Gulich., 2010, has performed numerous studies on a cavitation rig and reported correlations for cavitation inception and cavity length predictions.

In this paper, we study the influence of blade leading edge profiles, keeping all other parameters as identical, on the cavitation behavior of an impeller. Leading edge profiles such as blunt, circular, elliptic, and parabola are considered and the effect of different profiles on cavitation inception, bubble growth, cavity length and NPSH-3% head drop performance are investigated. Experiments are performed on a cavitation visualization test rig and complemented by two-phase computational fluid dynamic (CFD) modeling and analysis. To the authors' knowledge, this is the first study that takes an in depth look at the impeller leading edge profiles and their influence on the cavitation behavior of an impeller.

VISUALIZATION TEST RIG

The cavitation rig is designed to conduct visual studies of cavitation happening at the impeller eye. The visualization test rig is designed to simulate the suction geometry of a Between-Bearing (BB) style pump. Specifically the suction geometry is based on an existing, specific speed Ns = 1520 (nq = 29) design with a quasi symmetric inlet type. The suction specific speed for the original design is Nss = 10750 (S = 208). The suction area progression is based on internally established design rules. These rules have been validated by both prior experiment and CFD as providing a very uniform flow field into the impeller eye and an entry velocity less than 16 ft/sec (5m/sec).

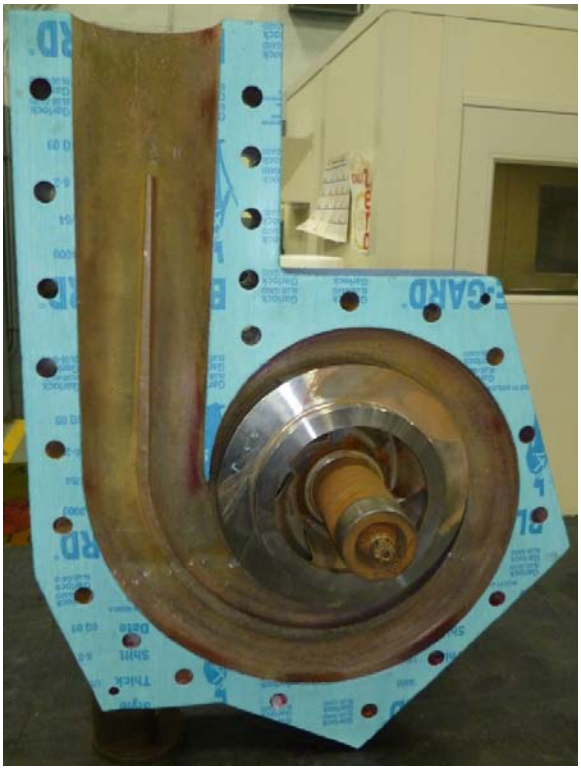

Figure 1: Split line detail of casing with the impeller in place on its carrier for the Test Rig.

Figure 2: Test Rig Assembly – looking through the viewing window

The test rig is constructed as a 2-part casing with a radial split along the center line of the discharge volute. Figure 1 shows the split plane detail with the impeller in place on its carrier. Cast construction via Rapid Prototype patterns is utilized in order to ensure accurate reproduction of the intended geometry. The cast material is aluminum in order to minimize the weight for handling purposes.

A transparent cover made of acrylic has been installed to allow an unrestricted view into the impeller eye during testing. Figure 2 shows the view through look out window with the impeller in place. Grid lines are drawn on the impeller suction surface at equal intervals to measure bubble growth and the extent of cavity development. The cover contains a steady bearing to stabilize the shaft movement and correctly simulate the BB pump type. Rotor support, sealing and drive are provided using a standard OH2 bearing frame adapted for the test rig using a shaft engineered for the purpose. The impellers being tested are mounted on a carrier that was in turn mounted to the shaft. The cross-sectional view of the test rig assembly is shown in Figure 3.

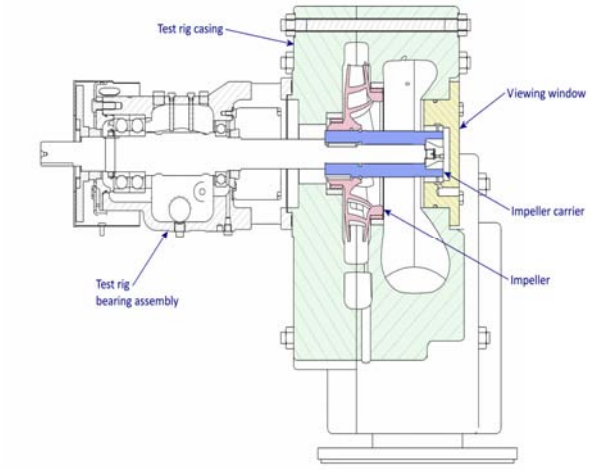

Figure 3: Visualization Test Rig Cross-sectional Assembly

VANE LEADING EDGE PROFILES

For the cavitation test rig, a single entry thru-shaft impeller has been utilized. The impeller has a standard front wear ring with clearances according to API 610 Table 6. The boiler-feed service impeller has a conventional design with 6 vanes created using our standard rules and process for impeller design. Onto this base design, several different vane leading edge treatments have been applied. The profiles used are:

- Blunt (flat face with rounded corners)
- Circular
- Elliptical
- Parabolic

The profile associated with each treatment is shown as a planar projection in Figure 4. The edge treatments are chosen to provide a representative range of profiles commonly used on impellers. All other parameters of the impeller design are held constant. The impellers have been manufactured by rapid investment casting techniques (pattern less manufacture) and the cast impellers using SLA rapid prototyping process are

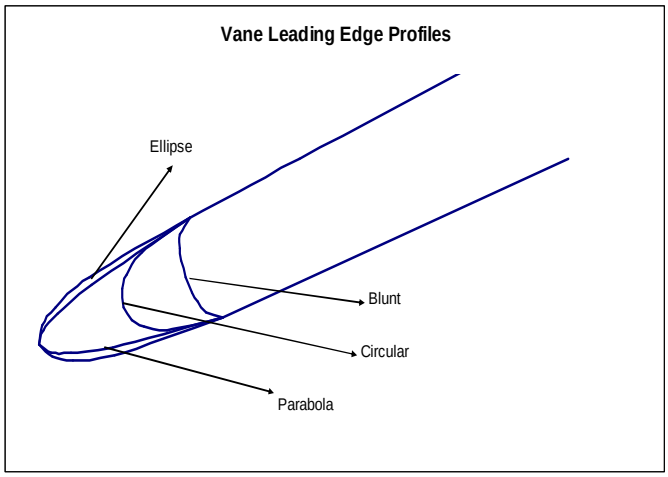

Figure 4: Different Vane Leading Edge Profiles

shown in Figure 5. The leading edge snapshots of the cast impellers highlighting the as-cast profiles can be noticed in Figure 5. By keeping the process and the manufacturer the same, conformity between each impeller casting has been assured.

Figure 5: Cast Impellers with different leading edge profiles

COMPUTATIONAL FLUID DYNAMICS

The computational study is conducted within the framework of the ANSYS-CFX solver, [ANSYS CFX-12.1, 2010]. The homogeneous two-phase mixture model is employed to model cavitation. The cavitation model is based on the Rayleigh-Plesset equation with source terms for the generation and destruction (vaporization and condensation) of vapor bubbles [Bakir et al., 2004]. The model solves for two-phases, vapor phase (α_{vapor}) and liquid phase (α_{water}), at each control volume location, with the sum of both phases equal to one ($\alpha_{vapor}+\alpha_{water}=1$) at each location. The basic assumption of the model is that all phases share the same velocity and a mixture equation is solved for the conservation of momentum. High resolution fluxes are chosen for the discretization of mean flow and turbulence equations. The shear stress transport (SST) turbulence model is used for modeling turbulence.

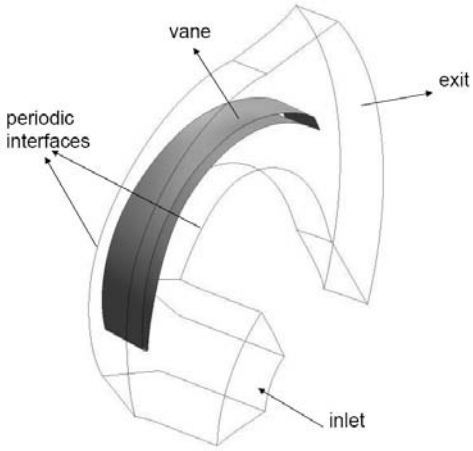

Figure 6: Single-passage CFD model for analysis

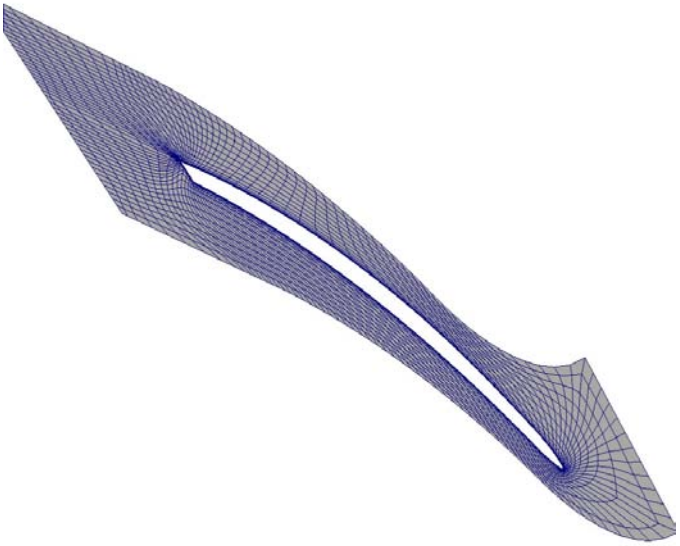

Figure 7: Mid-span Blade-to-blade grid: 241x35; (alternate i and j line removed in figure for clarity)

Simulations are performed for a single passage of the impeller geometry as shown in Figure 6. A 241x35x51 structured grid is generated, 241 points in the streamwise direction, 35 points blade-to-blade and 51 points from hub-to-shroud. The first point off the wall has a y^+ value less than 5 to

accurately resolve the boundary layer. Figures 7 shows snapshot of the grid a blade-to-blade segment. Though not shown here for lack of space, a grid refinement study is conducted with finer (481x69x101) and coarser (121x18x26) grids and, the current medium grid has been found to be sufficient for the analysis. For the analysis, no slip boundary conditions are applied at the hub, shroud and blade; total pressure is set at the inlet with the volume fraction of water as 1.0 and vapor as 0.0; mass flow rate is specified at the exit; rotational periodicity is applied at the periodic interfaces (passage boundaries) as shown in Figure 7. The inlet total pressure is gradually reduced to compute the head drop performance curves similar to a typical NPSH test run.

ANALYSIS CRITERIA

Head Drop Curves

The head drop cavitation curves summarize the drop in head for different cavitation criteria. Figure 9 shows the head drop performances of the impeller with parabola leading edge profile for different flow rates. The head drop curves for each flow rate are determined in a suction test at constant speed by successive reduction of the inlet pressure. The σ_1 and σ_3 criteria (or the $NPSH_1$ and $NPSH_3$ values) correspond to the 1% and 3% drop in head. Also, shown in Figure 9 is the head break-down point, the suction pressure beyond which there is a total decay in head production. Comparison of the head drop curves of the different leading edge profiles provides valuable information in the evaluation of $NPSH_1$ and $NPSH_3$ performances.

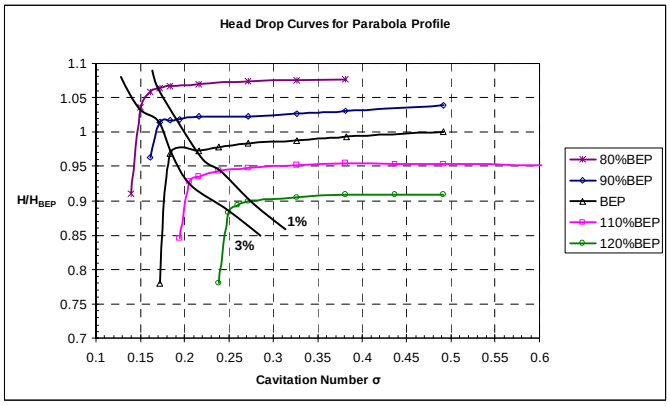

Figure 9: Head drop curves for Parabola profile at different flow rates and NPSHa

Cavitation Bubble Growth and Cavity Length

The cavity length or vapor cavity length (L_{cav}) represents the amount of developed cavitation and is an appropriate representation of the cavitation bubble growth and sheet cavitation. Figures 10, 11 and 12 show the extent of vapor cavity development at the impeller mid-span location for 1% head drop, 3% head drop and head break-down conditions. The blade loading (surface pressure distribution) is also plotted on the second y-axis to provide additional clarity on the head production at these various conditions. These Figures correspond to the BEP flow of the impeller with parabola leading edge profile.

Note that the cavity lengths in all the figures are non-dimensionalized by the streamwise blade chord length, ($L_{cav,nd}$). The inlet throat is located at about 35% of the blade chord length from the leading edge for all the blade geometries.

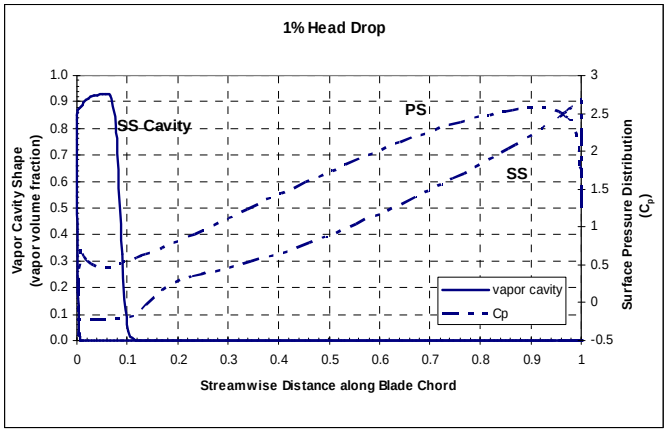

Figure 10: Vapor cavity shape and blade pressure distribution for Parabola profile at mid-span location near 1% head drop, σ_1 = 0.22

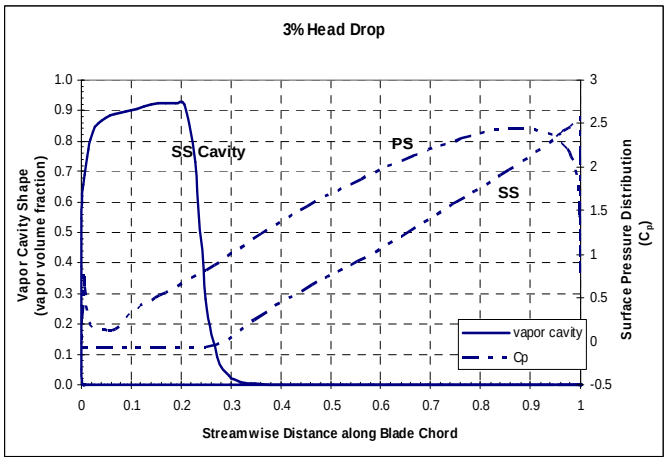

Figure 11: Vapor cavity shape and blade pressure distribution for Parabola profile at mid-span location near 3% head drop, σ_3 = 0.18

From Figures 10, 11 and 12, it can be observed that the flat portion of the blade loading curves on the suction surface (SS)

correspond to regions where the local static pressure has fallen below vapor pressure and represent cavitation zones. These cavitation zones are identified in the two-phase mixture model as regions occupied by vapor with the vapor volume fraction

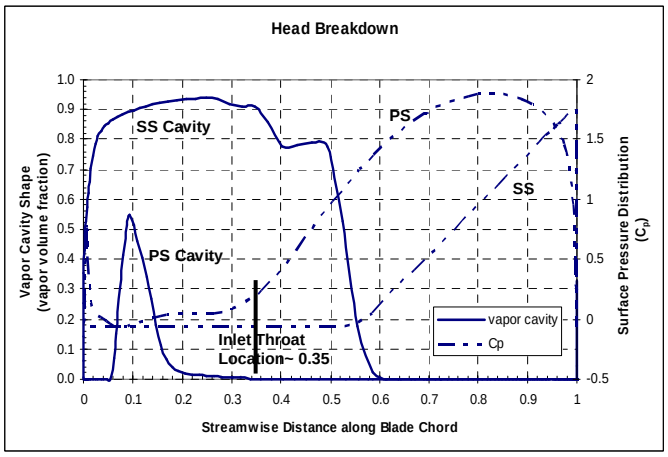

Figure 12: Vapor cavity shape and blade pressure distribution for Parabola profile at mid-span location showing head break-down, σ = 0.17

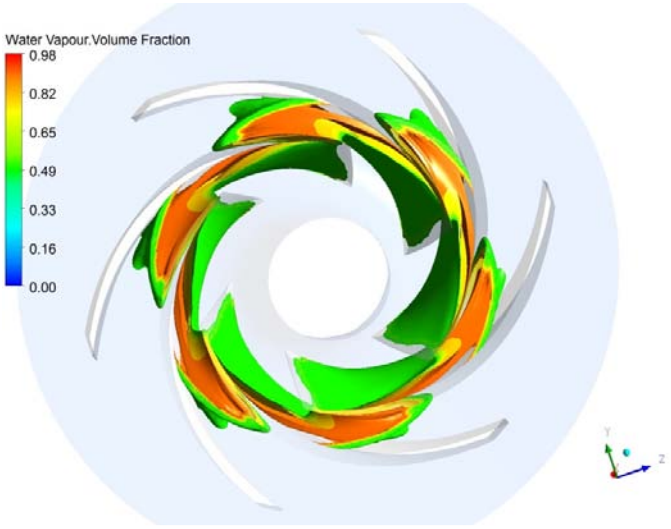

Figure 13: Iso-surfaces of vapor volume fraction showing sheet cavitation at head breakdown, σ = 0.17.

taking a value between 0 and 1; a value of 1 represents 100% of the volume is occupied by vapor alone and no water is present; a value of 0 represents 100% volume is occupied by water alone and no vapor is present; and a value between 0 and 1 represents fraction of volumes occupied by vapor. By plotting the vapor volume fraction as shown in Figures 10, 11 and 12, the shape of the vapor cavity and extent of cavity growth along the blade streamline can be studied. In Figures 10 and 11 for the 1% head drop and 3% head drop conditions, the vapor cavity has developed on the suction surface of the blade and has not completely blocked the impeller passage throat entrance. Also, the increase in cavity lengths with the reduction in cavitation coefficient can be verified. Figures 12 and 13 illustrate the interesting physics at head break down. Figure 13 shows the iso-surface contours of sheet cavitation and the extent of cavity development with cavitation bubbles blocking the impeller channels. From Figure 12, the extent of cavity development can be noticed with the presence of both suction surface (SS) and pressure surface (PS) cavitation zones. The cavity growth from the suction surface (SS) reaches the adjacent blade's pressure surface (PS) and blocks the impeller flow passages, thereby, leading to head break-down.

Comparison of the cavity lengths at different cavitation numbers for the leading edge profiles provides insights on the rate of bubble growth.

Impeller Life and Erosion Rate based on Cavity Length

A correlation for erosion rate can be derived based on the available NPSHa, fluid properties, material properties and the developed cavity lengths. Gulich [Gulich., 2010] has derived a relation that estimates the expected service life of impellers in hours given by

$$L_{I,\exp} = \frac{0.75 * e}{3600 E_R} \ \textit{hours} \qquad (1)$$

Where 'e' is the blade thickness in meter and 'E_R' is the erosion rate in meter/sec.

$$E_R = C_1 \left(\frac{\Delta p}{p_{ref}}\right)^3 \frac{F_{corr}}{F_{matl}} \left(\frac{L_{cav}}{L_{ref}}\right)^{2.83} \frac{a}{a_{ref}} \left(\frac{\quad}{\quad}_{ref}\right)^{0.36} \left(\frac{\quad}{\quad}_{ref}\right)^{0.44} \frac{1}{T_s} \qquad (2)$$

Here, C_1=5.4x10^{-24} W/m^2 is the cavitation constant for suction surface erosion; F_{corr} is the corrosion factor of the pumping fluid, F_{corr}=1.0 for fresh water; F_{matl} is the corrosion resistance factor of the impeller material based on the pumping fluid; L_{cav} is the cavity length in mm; a is the speed of sound in the liquid; α is the dissolved gas content in water; ρ is the saturated vapor density; T_s is the ultimate resilience of the material given by

$$T_s = T_s = \left(\frac{TensileStrength^2}{2 Young's Modulus}\right).$$

The reference values are,

$$L_{ref} = 10\text{mm},\ p_{ref} = 1\text{N/m}^2,\ a_{ref} = 1490\text{m/s}$$
$$_{ref} = 0.0173\text{kg/m}^3,\quad _{ref} = 24\text{ppm of dissolved gas} \qquad (3)$$

In equation (1), a 75 percent reduction in blade thickness constitutes the end of useful life of the impeller. In the above

equations, the fluid properties are characterized by the vapor density, corrosion factor, speed of sound and gas content. The material properties are characterized by the tensile strength and the cavitation resistance factor. The corrosion erosion resistance properties of various materials are tabulated in Schiavello and Visser., 2008.

RESULTS AND DISCUSSIONS

The head drop performances of the different leading edge profiles are shown in Figures 15, 16, 17 and 18. The test data from the cavitation rig have also been plotted along with the data from CFD analyses. For all the flow rates, it can be observed that there is a good correlation between the CFD analysis and test data. The CFD predictions follow the trend of the experimental data. From the Figures, it can be deduced that the best $NPSH_1$ and the $NPSH_3$ performances for the various flow rates are by the impeller with parabolic leading edge, followed by the ellipse profile with the circular and blunt profiles trailing them. As expected, the worst performance is observed in the blunt profile because of the shock and entrance losses introduced by the sharp leading edge contour.

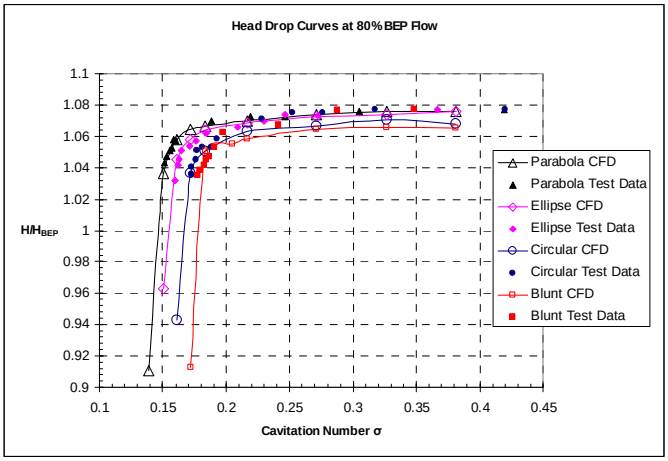

Figure 14: Head drop curves for different leading edge profiles at 80% BEP Flow

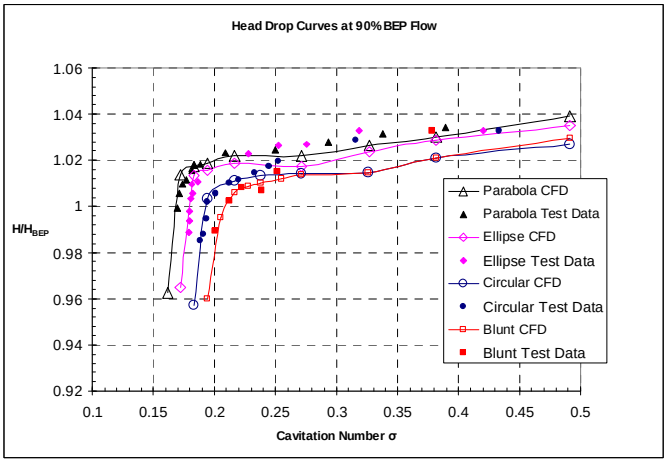

Figure 15: Head drop curves for different leading edge profiles at 90% BEP Flow.

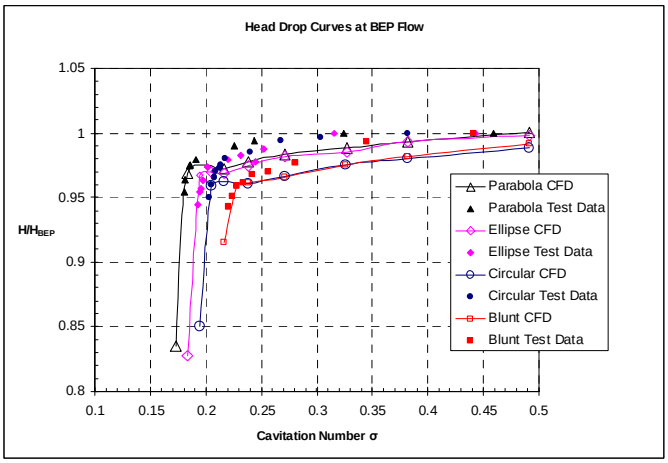

Figure 16: Head drop curves for different leading edge profiles at BEP Flow

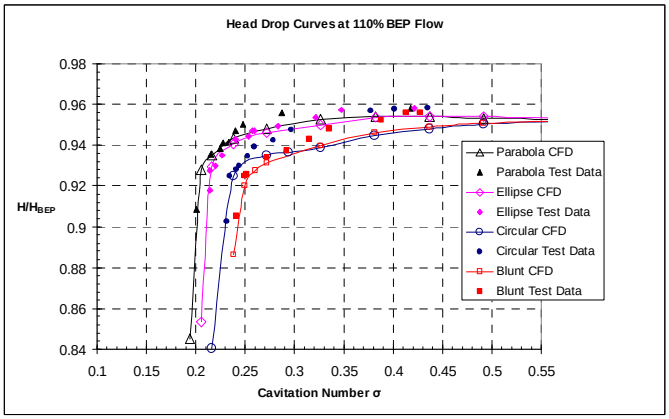

Figure 17: Head drop curves for different leading edge profiles at 110% BEP Flow

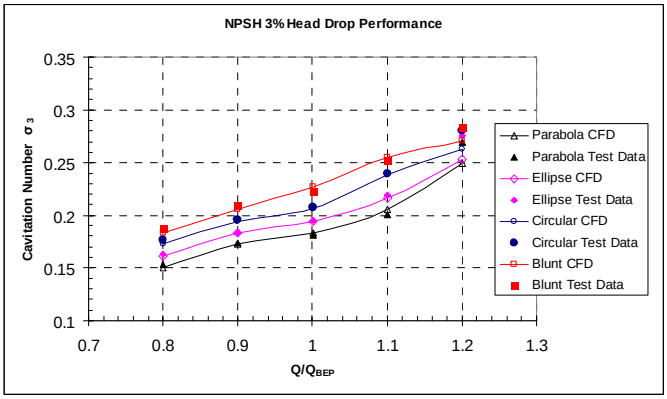

Figure 18: NPSH-3% Head Drop Performance.

For additional clarity, the NPSH-3% head drop performance is plotted in Figure 18. It can be observed that there is a 20% difference in NPSHr values between the parabola and blunt profiles at all flow rates except at 120%BEP flow, with the values for rest of profiles falling in between. At 120% BEP flow, the casing effects dominate the flow with suction recirculation and flow blockage at the impeller eye. Additionally, the incidence is too large at the blade leading edge for the profiles to have any influence, with the entrance shock losses being significant. The deviation in NPSH values between the CFD and experiments at 120% BEP flow can be attributed to the CFD analysis not taking into account the effects of casing as only a single passage impeller analysis has been performed.

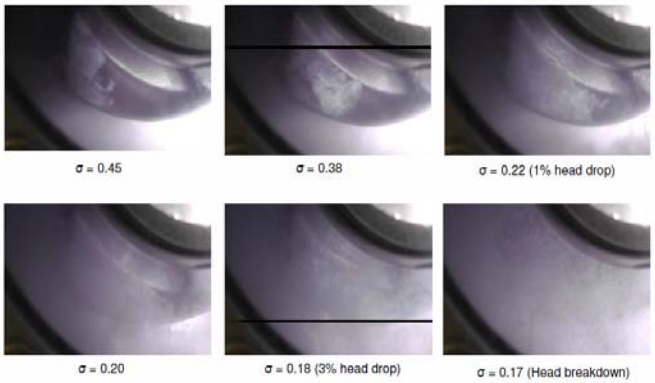

Figure 19: Cavitation Development at BEP flow in the impeller with Parabola profile as suction pressure is reduced.

Figure 19 shows instantaneous snapshots of bubble growth and cavitation development that were taken during a NPSH run at the cavitation rig. The pictures show the growth of vapor cavity for different inlet suction pressures during the NPSH test. The extent of vapor cavity development along the blade suction surface and the corresponding blockage in the blade passage at different phases of cavitation can be clearly observed.

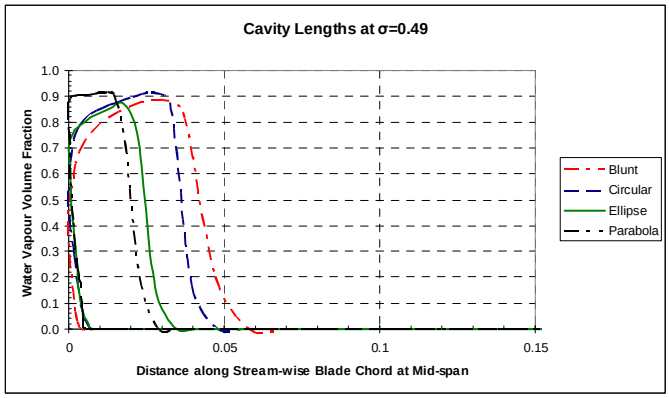

Figure 20: Vapor Cavity Lengths σ=0.49; BEP flow at mid-span location.

The cavity lengths for different values of cavitation coefficient are compared in Figures 21, 22 and 23. These plots compare the extent of vapor cavity along the streamwise chord of the blade at mid-span location. Note that the cavity lengths in the figures are non-dimensionalized by the streamwise blade chord length. From the Figures, it can be noticed that the cavity lengths are the shortest for the parabola profile with the blunt profile faring badly.

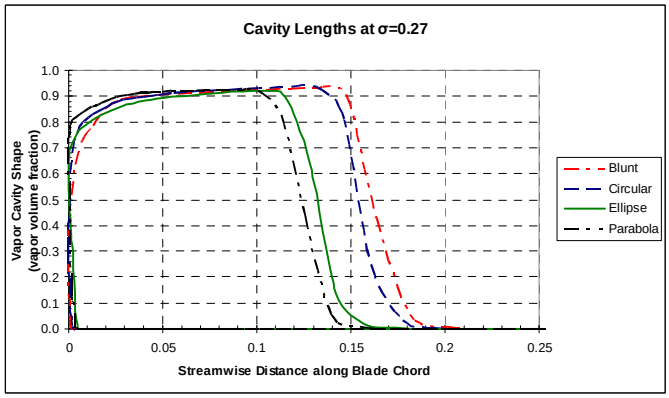

Figure 21: Vapor Cavity Lengths for σ=0.27; BEP flow at mid-span location.

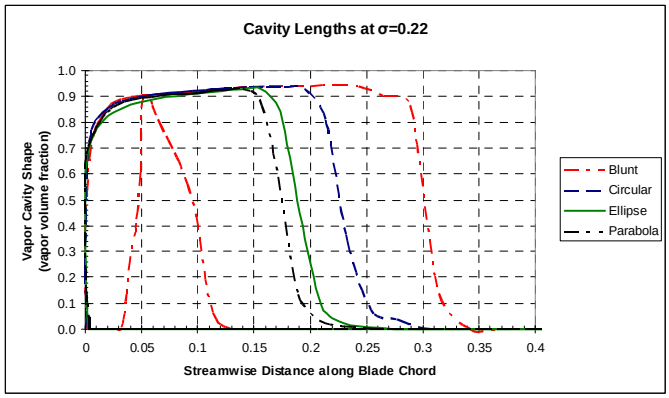

Figure 22: Vapor Cavity Lengths for σ=0.22; BEP flow at mid-span location.

The growth or increase in vapor cavity lengths at reduced values of σ can be noticed. In Figure 23 for σ=0.22, the blunt profile is approaching breakdown with the vapor cavity extending to the pressure surface of the adjacent blade. The cavity lengths for the ellipse profile follow the parabola profile closely and are slightly larger compared to the corresponding lengths of the parabola profile.

Figures 23, 24, 25 and 26 plot the extent of cavity lengths, with respect to different cavitation criteria for various flow rates. Again, the shortest cavity lengths can be observed for the parabola profile across all the flow rates, followed by the elliptical profile.

The expected service life of impellers for different materials of construction are reported in Tables 1 and 2 for σ = 0.27 and σ = 0.22. The values in Tables 1 and 2 are calculated using equation (1) with the pump operating at BEP flow and pumping fresh water that has a dissolved gas content of 23ppm at 25^0 C. The cavitation numbers σ = 0.27 and σ = 0.22 represent two different available NPSH scenarios; for the parabola profile with 3% head drop occurring at σ = 0.18, the NPSH values associated with σ = 0.27 and σ = 0.22 represent 1.5 and 1.2 times NPSH margin.

From the tables, it can be deduced that for a given material of construction the developed vapor cavity length has a direct impact on impeller life. The parabola profile with the shortest cavity lengths have the least cavitation related damage and longer impeller service life compared to the other profiles. At σ = 0.27, the service life of impeller with parabola profile is twice the service life of the impeller with blunt profile. At a much lower available NPSH for σ = 0.22, the service life of impeller with parabola profile is three times the service life of the impeller with blunt profile with the other configurations falling in between.

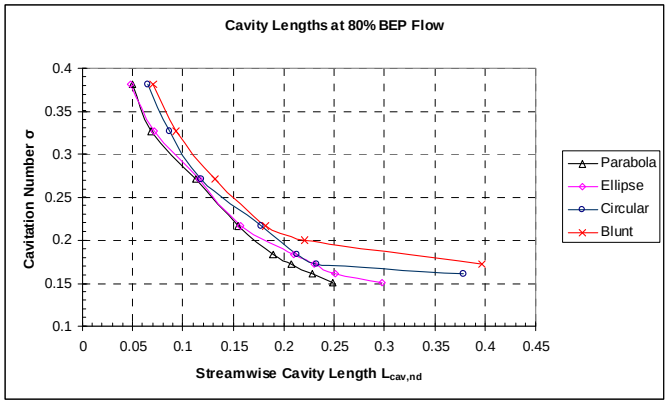

Figure 23: Cavitation bubble growth for different leading edge profiles as NPSH available is reduced; 80% BEP flow at mid-span location

Table 1: Expected service Life of Impeller in hours running at BEP flow with σ = 0.27 and pumping fresh water with dissolved gas content of 23ppm at 25^0 C with inlet eye velocity, U1= 30.4m/s (99.7ft/s)

Impeller Material	BHN	Impeller Life (hours)			
		Parabola	Ellipse	Circular	Blunt
Cast Carbon Steel (Ferritic)	156	20436	14659	10421	9705
Cast CF3M 316L(Austenitic)	170	32697	23455	16674	15528
Ferralium 255 (Duplex)	255	46518	33369	23723	22092
Cast CA6NM (Martenistic)	262	32023	22971	16631	15208

Table 2: Expected service Life of Impeller in hours running at BEP flow with σ = 0.22 and pumping fresh water with dissolved gas content of 23ppm at 25^0 C with inlet eye velocity, U1= 30.4m/s (99.7ft/s)

Impeller Material	BHN	Impeller Life (hours)			
		Parabola	Ellipse	Circular	Blunt
Cast Carbon Steel (Ferritic)	156	13113	9840	5848	4060
Cast CF3M 316L(Austenitic)	170	20982	15745	9357	6500
Ferralium 255 (Duplex)	255	29850	22400	13312	9248
Cast CA6NM (Martenistic)	262	20549	15420	9164	6366

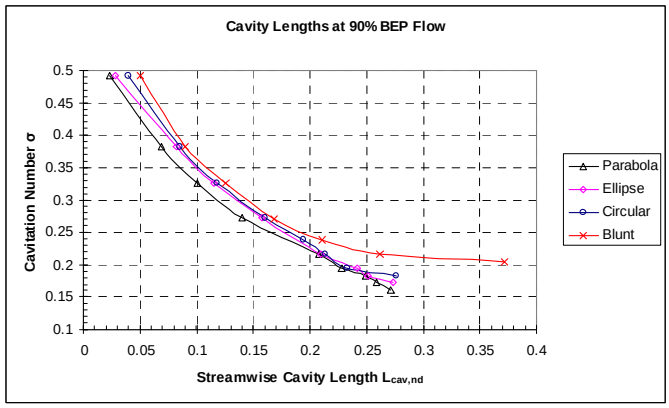

Figure 24: Cavitation bubble growth for different leading edge profiles as NPSH available is reduced; 90% BEP flow at mid-span location

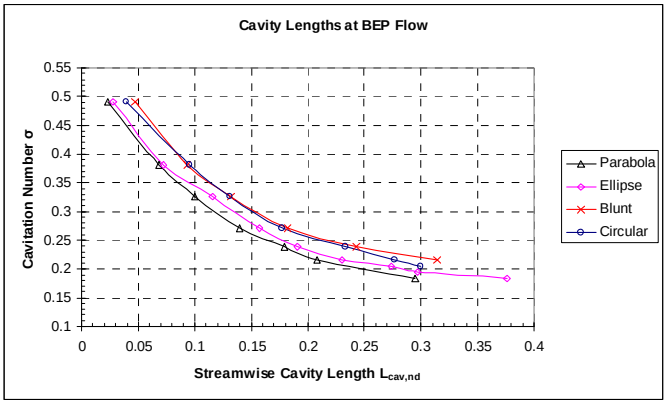

Figure 25: Cavitation bubble growth for different leading edge profiles as NPSH available is reduced; BEP flow at mid-span location

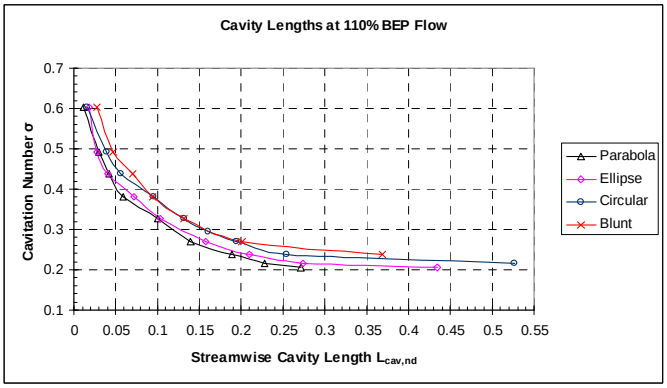

Figure 26: Cavitation bubble growth for different leading edge profiles as NPSH available is reduced; 110%BEP flow at mid-span location

SUMMARY AND CONCLUSIONS

The cavitation behavior and suction performance of a pump are largely influenced by geometric factors at the impeller eye such as, the inlet and hub diameters, blade inlet angles and incidence to upstream flow, blade number and thickness, blade passage throat area, surface roughness, blade leading edge profiling, etc. In this paper, the influence of blade leading edge profiles on the cavitation behavior of an impeller has been studied keeping all other parameters as identical. Leading edge profiles such as blunt, circular, elliptic, and parabola have been investigated. The head drop performances and cavitation bubble growth at different flow rates are studied on a cavitation visualization test rig and also, using computational fluid dynamic (CFD) analyses with a homogeneous two-phase mixture model.

The leading edge profile with parabola definition has the best overall performance and as expected, the blunt profile has the worst overall performance. The head drop performance curves have clearly demonstrated the superior $NPSH_3$ performance of the parabola profile at the flow ranges that are of major interest to the pump users. The growth of the vapor bubbles and length of sheet cavity is considerably smaller for the parabola profile, and will result in lesser cavitation damage and longer impeller life.

From the head drop performance curves and cavity lengths, it can be concluded that the suction performance of an impeller can be improved by adopting the parabola profile provided the mechanical and manufacturing constraints on leading edge vane thickness can be satisfied. The elliptical profile performs second best and should be the default profile of choice for the leading edge as the mechanical and manufacturing constraints on blade leading edge thickness can be easily met with this profile.

NOMENCLATURE

H_{BEP} = non-cavitating head at BEP flow
$NPSH_A$ = available net positive suction head
$NPSH_1$ = net positive suction head at 1% head drop
$NPSH_3$ = net positive suction head at 3% head drop
$NPSH_i$ = incipient net positive suction head
p_{Sat} = saturation vapor pressure of water
p_1 = static pressure at impeller inlet
p_{01} = total pressure at impeller inlet
ρ = density of water
σ = cavitation number (= $(2gNPSH_x)/ u_1^2$)
σ_i = incipient cavitation number
σ_1 = cavitation number at 1% head drop
σ_3 = cavitation number at 3% head drop
L_{cav} = vapor cavity length (or cavitation bubble length) along the streamwise blade chord
L_{bc} = length of streamwise blade chord
$L_{cav,nd}$ = non-dimensionalized vapor cavity length (=L_{cav} / L_{bc})
u_1 = peripheral velocity at impeller eye (m/sec)
SS = suction surface
PS = pressure surface
C_p = surface pressure distribution coefficient

REFERENCES

1. ANSYS-12.1 CFX Solver Theory Guide, 2010.

2. Bakir, F., Rey, R., Gerber, A. G., Belamri, T., and Hutchinson, B., 2004, Numerical and Experimental Investigations of the Cavitating Behavior of an Inducer, ***International Journal of Rotating Machinery***, Vol. 10, pp 15—25, 2004.

3. Dupont, P., 2001, Numerical Prediction of Cavitation in Pumps, ***Proceedings of 18th International Pump Users Symposium,***

2001, Turbomachinery Laboratory, Department of Mechanical Engineering, Texas A&M University, College Station, TX, pp. 59—64.

4. Gulich, J.-F., 2010, Centrifugal Pumps, Third Edition-English, Springer-Verlag Publishers 2008.

5. Hergt, P., Nicklas, A., Mollenkopf, G., and Brodersen, S., 1996, The Suction Performance of Centrifugal Pumps Possibilities and Limits of Improvements, ***Proceedings of the 13th International Pump Users Symposium, 1996***, Turbomachinery Laboratory, Department of Mechanical Engineering, Texas A&M University, College Station, TX, pp. 13—25.

6. Kovats, A., 1964, Design and Performance of Centrifugal and Axial Flow Pumps and Compressors, Pergamon Press, 1964.

7. Palgrave, R., and Cooper, P., 1986, Visual Studies of Cavitation in Pumping Machinery, ***Proceedings of the 3rd International Pump Users Symposium, 1986,*** Turbomachinery Laboratory, Department of Mechanical Engineering, Texas A&M University, College Station, TX.

8. Schiavello, B., Arisawa, T., and Marenco, G., 1989, Flow Visualization – A Design Tool to Improve Pump Cavitation Performance, ***Transport phenomena in rotating machinery: part I of the proceedings of the Second International Symposium on Transport Phenomena, Dynamics, and Design of Rotating Machinery,*** 1989.

9. Schiavello, B., and Visser, F. C., 2008, Pump Cavitation – Various NPSHr Criteria, NPSHa Margins, and Impeller Life Expectancy, ***Proceedings of the 24th International Pump Users Symposium, 2008***, Turbomachinery Laboratory, Department of Mechanical Engineering, Texas A&M University, College Station, TX.

10. Sloteman, D.P., 1995, Avoiding cavitation in the suction stage of high energy pumps, ***World Pumps***, issue 348, 1995, pp. 40—48.

ACKNOWLEDGEMENTS

Special thanks to David Skinner for his resourcefulness and help in the completion of several key tasks for the project. Acknowledgements to Louis Jordan and Dennie Fenner for help in running the test rig.